

# SHAPE RECONSTRUCTION IN LINEAR ELASTICITY: ONE-STEP LINEARIZATION AND MONOTONICITY-BASED REGULARIZATION

SARAH EBERLE\* AND BASTIAN HARRACH†

**Abstract.** We deal with the shape reconstruction of inclusions in elastic bodies. Therefore, we review the monotonicity methods introduced in a former work of the authors. These monotonicity methods build the basis for the improvement of the standard one-step linearization method. The one-step linearization method consists of solving a minimization problem with standard regularization techniques, which is commonly used in practice but builds only a heuristical approach since there is no proven theory of its convergence. In contrary, the monotonicity-based regularization, where we introduce constraints for the minimization problem via the monotonicity methods, has a rigorously proven theory, i.e., we prove the existence and uniqueness of a minimizer as well as the convergence of the method for noisy data. Finally, we present numerical experiments.

**Key words.** linear elasticity, inverse problem, shape reconstruction, one-step linearization method, monotonicity-based regularization

**AMS subject classifications.** 35R30, 65M32

**1. Introduction.** The main motivation is the non-destructive testing of elastic structures, such as is required for material examinations, in exploration geophysics, and for medical diagnostics (elastography). From a mathematical point of view, this constitutes an inverse problem since we have only measurement data on the boundary and not inside of the elastic body. This problem is highly ill-posed, since even the smallest measurement errors can completely falsify the result.

There are several authors who deal with the theory of the inverse problem of elasticity. For the two dimensional case, we refer the reader to [12, 19, 13, 15]. In three dimensions, [20, 21] and [7] gave the proof for uniqueness results for both Lamé coefficients under the assumption that  $\mu$  is close to a positive constant. [2, 3] proved the uniqueness for partial data, where the Lamé parameters are piecewise constant and some boundary determination results were shown in [18, 20, 15].

Further on, solution methods applied so far for the inverse problem, which will be solved in this paper, were presented in the following works: In [22] and [23], the time-independent inverse problem of linear elasticity is solved by means of the adjoint method and the reconstruction is simulated numerically. In addition, [24] deals with the coupling of the state and adjoint equation and added two variants of residual-based stabilization to solve the inverse linear elasticity problem for incompressible plane stress. A boundary element-Landweber method for the Cauchy problem in stationary linear elasticity was investigated in [17]. In [11], the stationary inverse problem was solved by means of a Landweber iteration as well and numerical examples were presented. Reciprocity principles for the detection of cracks in elastic bodies were investigated, for example, in [1] and [25] or more recently in [8]. By means of a regularization approach, a stationary elastic inverse problem is solved in [14] and applied in numerical examples. [16] introduces a regularized boundary element method.

---

\*eberle@math.uni-frankfurt.de, Institute of Mathematics, Goethe-University Frankfurt, Frankfurt am Main, Germany (corresponding author)

†harrach@math.uni-frankfurt.de, Institute of Mathematics, Goethe-University Frankfurt, Frankfurt am Main, Germany

Finally, we want to mention the monotonicity methods for linear elasticity developed by the authors of this paper in [5].

In this paper, the key issue of the shape reconstruction of inclusions is the monotonicity property of the corresponding Neumann-to-Dirichlet operator (see [26, 27]). These monotonicity properties were also applied for electrical impedance tomography (see, e.g., [10]) and for linear elasticity in [6]. Further on, the so-called monotonicity tests as introduced in [5] build the basis for our current work.

The outline of the paper is as follows: We start with the introduction of the problem statement. After that, we take a look at the standard one-step linearization method. We would like to point out that this method is only a heuristic approach, but forms the basis for the monotonicity-based regularization. Similar to the linearized monotonicity test, we also consider the Fréchet derivative, which approximates the difference between two Neumann-to-Dirichlet operators. We want to determine the difference between an unknown Lamé parameter pair  $(\lambda, \mu)$  and that of the known background  $(\lambda_0, \mu_0)$  and formulate a minimization problem. In order to solve this minimization problem, regularization parameters are introduced, which can only be determined heuristically. For this purpose, for example, a parameter study can be carried out. Overall, this heuristic approach leads to reconstructions of the unknown inclusions without a rigorous theory. In Section 4, we focus on the monotonicity-based regularization and start with a short overview of the linearized monotonicity tests. The idea of the “new kind” of regularization is to introduce conditions for the parameters / inclusions to be reconstructed for the minimization problem, which are based on the monotonicity properties of the Neumann-to-Dirichlet operator and the monotonicity tests. Further on, we will prove that there exists a unique minimizer for this problem and that we obtain convergence even for noisy data. Finally, we present numerical examples.

**2. Problem Statement.** We start with the introduction of the problems of interest, e.g., the *direct* as well as *inverse problem* of stationary linear elasticity.

Let  $\Omega \subset \mathbb{R}^d$  ( $d = 2$  or  $3$ ) be a bounded and connected open set with Lipschitz boundary  $\partial\Omega = \Gamma = \overline{\Gamma_D} \cup \Gamma_N$ ,  $\Gamma_D \cap \Gamma_N = \emptyset$ , where  $\Gamma_D$  and  $\Gamma_N$  are the corresponding Dirichlet and Neumann boundaries. We assume that  $\Gamma_D$  and  $\Gamma_N$  are relatively open and connected. Further on, let  $u : \Omega \rightarrow \mathbb{R}^d$  be the displacement vector,  $\mu, \lambda : \Omega \rightarrow L_+^\infty(\Omega)$  the Lamé parameters,  $\hat{\nabla}u = \frac{1}{2}(\nabla u + (\nabla u)^T)$  the symmetric gradient,  $n$  is the normal vector pointing outside of  $\Omega$ ,  $g \in L^2(\Gamma_N)^d$  the boundary force and  $I$  the  $d \times d$ -identity matrix. For the following, we define the divergence of a matrix  $A \in \mathbb{R}^{d \times d}$  via  $\nabla \cdot A = \sum_{i,j=1}^d \frac{\partial A_{ij}}{\partial x_j} e_i$ , where  $e_i$  is a unit vector and  $x_j$  a component of a vector from  $\mathbb{R}^d$ .

The boundary value problem of linear elasticity (*direct problem*) is that  $u \in H^1(\Omega)^d$  solves

$$(2.1) \quad \nabla \cdot (\lambda(\nabla \cdot u)I + 2\mu\hat{\nabla}u) = 0 \quad \text{in } \Omega,$$

$$(2.2) \quad (\lambda(\nabla \cdot u)I + 2\mu\hat{\nabla}u)n = g \quad \text{on } \Gamma_N,$$

$$(2.3) \quad u = 0 \quad \text{on } \Gamma_D.$$

From a physical point of view, this means that we deal with an elastic test body  $\Omega$  which is fixed (zero displacement) at  $\Gamma_D$  (Dirichlet condition) and apply a force  $g$  on  $\Gamma_N$  (Neumann condition). This results in the displacement  $u$ , which is measured on the boundary  $\Gamma_N$ .

The equivalent weak formulation of the boundary value problem (2.1)-(2.3) is that  $u \in \mathcal{V}$  fulfills

$$(2.4) \quad \int_{\Omega} 2\mu \hat{\nabla} u : \hat{\nabla} v + \lambda \nabla \cdot u \nabla \cdot v \, dx = \int_{\Gamma_N} g \cdot v \, ds \quad \text{for all } v \in \mathcal{V},$$

where  $\mathcal{V} := \left\{ v \in H^1(\Omega)^d : v|_{\Gamma_D} = 0 \right\}$ .

We want to remark that for  $\lambda, \mu \in L_+^\infty(\Omega)$  the existence and uniqueness of a solution to the variational formulation (2.4) can be shown by the Lax-Milgram theorem (see e.g., in [4]).

Measuring boundary displacements that result from applying forces to  $\Gamma_N$  can be modeled by the Neumann-to-Dirichlet operator  $\Lambda(\lambda, \mu)$  defined by

$$\Lambda(\lambda, \mu) : L^2(\Gamma_N)^d \rightarrow L^2(\Gamma_N)^d : \quad g \mapsto u|_{\Gamma_N},$$

where  $u \in \mathcal{V}$  solves (2.1)-(2.3).

This operator is self-adjoint, compact and linear (see Corollary 1.1 from [5]). Its associated bilinear form is given by

$$(2.5) \quad \langle g, \Lambda(\lambda, \mu)h \rangle = \int_{\Omega} 2\mu \hat{\nabla} u_{(\lambda, \mu)}^g : \hat{\nabla} u_{(\lambda, \mu)}^h + \lambda \nabla \cdot u_{(\lambda, \mu)}^g \nabla \cdot u_{(\lambda, \mu)}^h \, dx,$$

where  $u_{(\lambda, \mu)}^g$  solves the problem (2.1)-(2.3) and  $u_{(\lambda, \mu)}^h$  the corresponding problem with boundary force  $h \in L^2(\Gamma_N)^d$ .

Another important property of  $\Lambda(\lambda, \mu)$  is its Fréchet differentiability (for the corresponding proof see Lemma 2.3 in [5]). For directions  $\hat{\lambda}, \hat{\mu} \in L^\infty(\Omega)$ , the derivative

$$\Lambda'(\lambda, \mu)(\hat{\lambda}, \hat{\mu}) : L^2(\Gamma_N)^d \rightarrow L^2(\Gamma_N)^d$$

is the self-adjoint compact linear operator associated to the bilinear form

$$\langle \Lambda'(\lambda, \mu)(\hat{\lambda}, \hat{\mu})g, h \rangle = - \int_{\Omega} 2\hat{\mu} \hat{\nabla} u_{(\lambda, \mu)}^g : \hat{\nabla} u_{(\lambda, \mu)}^h + \hat{\lambda} \nabla \cdot u_{(\lambda, \mu)}^g \nabla \cdot u_{(\lambda, \mu)}^h \, dx.$$

Note that for  $\hat{\lambda}_0, \hat{\lambda}_1, \hat{\mu}_0, \hat{\mu}_1 \in L^\infty(\Omega)$  with  $\hat{\lambda}_0 \leq \hat{\lambda}_1$  and  $\hat{\mu}_0 \leq \hat{\mu}_1$  we obviously have

$$(2.6) \quad \Lambda'(\lambda, \mu)(\hat{\lambda}_0, \hat{\mu}_0) \geq \Lambda'(\lambda, \mu)(\hat{\lambda}_1, \hat{\mu}_1),$$

in the sense of operator definiteness (aka Loewner order).

The *inverse problem* we consider here is the following

*Find  $(\lambda, \mu)$  knowing the Neumann-to-Dirichlet operator  $\Lambda(\lambda, \mu)$ .*

Next, we take a look at the discrete setting. Let the Neumann boundary  $\Gamma_N$  be the union of the patches  $\Gamma_N^{(l)}$ ,  $l = 1, \dots, M$ , which are assumed to be relatively open and connected, such that  $\overline{\Gamma_N} = \bigcup_{l=1}^M \overline{\Gamma_N^{(l)}}$ ,  $\Gamma_N^{(i)} \cap \Gamma_N^{(j)} = \emptyset$  for  $i \neq j$  and we consider the following problem:

$$(2.7) \quad \nabla \cdot (\lambda(\nabla \cdot u)I + 2\mu \hat{\nabla} u) = 0 \quad \text{in } \Omega,$$

$$(2.8) \quad (\lambda(\nabla \cdot u)I + 2\mu \hat{\nabla} u) n = g_l \quad \text{on } \Gamma_N^{(l)},$$

$$(2.9) \quad (\lambda(\nabla \cdot u)I + 2\mu \hat{\nabla} u) n = 0 \quad \text{on } \Gamma_N^{(i)}, \quad i \neq l,$$

$$(2.10) \quad u = 0 \quad \text{on } \Gamma_D,$$

where  $g_l$ ,  $l = 1, \dots, M$ , denote the  $M$  given boundary forces applied to the corresponding patches  $\Gamma_N^{(l)}$ . In order to discretize the Neumann-to-Dirichlet operator, we apply a boundary force  $g_l$  on the patch  $\Gamma_N^{(l)}$  and set

$$\Lambda_l^{(k)}(\lambda, \mu) := \int_{\Gamma_N^{(l)}} g_l \cdot u^{(k)} ds$$

(cf. (2.4) and (2.5)), where  $u^{(k)}$  solves the corresponding boundary value problem (2.7)-(2.10) with boundary force  $g_k$ .

In practice, we use orthonormal vectors  $g_l \in L^2(\Gamma_N)^d$  in order to discretize  $\Lambda(\lambda, \mu)$ .

For the unknown Lamé parameters  $(\lambda, \mu)$ , we obtain a full matrix

$$\mathbf{\Lambda}(\lambda, \mu) = \left( \Lambda_l^{(k)}(\lambda, \mu) \right)_{k,l=1,\dots,M}.$$

**3. Standard One-step Linearization Methods.** In this section we take a look at one-step linearization methods. We want to remark that these methods are only a heuristical approach but commonly used in practice.

We compare the matrix of the discretized Neumann-to-Dirichlet operator  $\mathbf{\Lambda}(\lambda, \mu)$  with  $\mathbf{\Lambda}(\lambda_0, \mu_0)$  for some reference Lamé parameter  $(\lambda_0, \mu_0)$  in order to reconstruct the difference  $(\lambda, \mu) - (\lambda_0, \mu_0)$ . Thus, we apply a single linearization step

$$\mathbf{\Lambda}'(\lambda_0, \mu_0)((\lambda, \mu) - (\lambda_0, \mu_0)) \approx \mathbf{\Lambda}(\lambda, \mu) - \mathbf{\Lambda}(\lambda_0, \mu_0),$$

where

$$\mathbf{\Lambda}'(\lambda_0, \mu_0) : L^\infty(\Omega)^2 \rightarrow \mathbb{R}^{M \times M}$$

is the Fréchet derivative which maps  $(\hat{\lambda}, \hat{\mu}) \in L^\infty(\Omega)^2$  to

$$- \left( \int_{\Omega} \hat{\lambda} \left( \nabla \cdot u_{(\lambda_0, \mu_0)}^{(k)} \right) \left( \nabla \cdot u_{(\lambda_0, \mu_0)}^{(l)} \right) + \hat{\mu} \left( \hat{\nabla} u_{(\lambda_0, \mu_0)}^{(k)} \right) : \left( \hat{\nabla} u_{(\lambda_0, \mu_0)}^{(l)} \right) dx \right)_{1 \leq k, l \leq M}.$$

For the solution of the problem, we discretize the reference domain  $\overline{\Omega} = \bigcup_{j=1}^p \overline{B_j}$  into

$p$  disjoint pixel  $\mathcal{B}_j$ , where each  $\mathcal{B}_j$  is assumed to be open,  $\Omega \setminus \mathcal{B}_j$  is connected and  $\mathcal{B}_j \cap \mathcal{B}_i = \emptyset$  for  $j \neq i$ . We make a piecewise constant ansatz for  $(\kappa, \nu) \approx (\lambda, \mu) - (\lambda_0, \mu_0)$  via

$$(3.1) \quad \kappa(x) = \sum_{j=1}^p \kappa_j \chi_{\mathcal{B}_j}(x) \quad \text{and} \quad \nu(x) = \sum_{j=1}^p \nu_j \chi_{\mathcal{B}_j}(x),$$

where  $\chi_{\mathcal{B}_j}$  is the characteristic function w.r.t. the pixel  $\mathcal{B}_j$  and set

$$\boldsymbol{\kappa} = (\kappa_j)_{j=1}^p \in \mathbb{R}^p \quad \text{and} \quad \boldsymbol{\nu} = (\nu_j)_{j=1}^p \in \mathbb{R}^p.$$

This approach leads to the linear equation system

$$(3.2) \quad \mathbf{S}^\lambda \boldsymbol{\kappa} + \mathbf{S}^\mu \boldsymbol{\nu} = \mathbf{V},$$

where  $\mathbf{V}$  and the columns of the sensitivity matrices  $\mathbf{S}^\lambda$  and  $\mathbf{S}^\mu$  contain the entries of  $\Lambda(\lambda, \mu) - \Lambda(\lambda_0, \mu_0)$  and the discretized Fréchet derivative for a given  $\mathcal{B}_j$  for  $j = 1, \dots, p$ , respectively. Here, we have

$$(3.3) \quad \mathbf{V} = (V_i)_{i=1}^{M^2} \in \mathbb{R}^{M^2}, \quad V_{(l-1)M+k} = \Lambda_l^{(k)}(\lambda_0, \mu_0) - \Lambda_l^{(k)}(\lambda, \mu),$$

$$(3.4) \quad \mathbf{S}^\lambda = (S_{ij}^\lambda) \in \mathbb{R}^{M^2, p}, \quad S_{(l-1)M+k, j}^\lambda = \int_{\mathcal{B}_j} \left( \nabla \cdot u_{(\lambda_0, \mu_0)}^{(k)} \right) \left( \nabla \cdot u_{(\lambda_0, \mu_0)}^{(l)} \right) dx,$$

$$(3.5) \quad \mathbf{S}^\mu = (S_{ij}^\mu) \in \mathbb{R}^{M^2, p}, \quad S_{(l-1)M+k, j}^\mu = \int_{\mathcal{B}_j} 2 \left( \hat{\nabla} u_{(\lambda_0, \mu_0)}^{(k)} \right) : \left( \hat{\nabla} u_{(\lambda_0, \mu_0)}^{(l)} \right) dx.$$

Solving (3.2) results in a standard minimization problem for the reconstruction of the unknown parameters. In order to determine suitable parameters  $(\kappa, \nu)$ , we regularize the minimization problem, so that we have

$$(3.6) \quad \left\| \begin{pmatrix} \mathbf{S}^\lambda & \mathbf{S}^\mu \end{pmatrix} \begin{pmatrix} \boldsymbol{\kappa} \\ \boldsymbol{\nu} \end{pmatrix} - \mathbf{V} \right\|_2^2 + \omega \|\boldsymbol{\kappa}\|_2^2 + \tau \|\boldsymbol{\nu}\|_2^2 \rightarrow \min!$$

with  $\omega$  and  $\tau$  as regularization parameters. For solving this minimization problem we consider the normal equation

$$\mathbf{A}^T \mathbf{A} \begin{pmatrix} \boldsymbol{\kappa} \\ \boldsymbol{\nu} \end{pmatrix} = \mathbf{A}^T \begin{pmatrix} \mathbf{V} \\ \mathbf{0} \\ \mathbf{0} \end{pmatrix}$$

$$\text{with } \mathbf{A} = \begin{pmatrix} \mathbf{S}^\lambda & | & \mathbf{S}^\mu \\ \omega \mathbf{I} & | & \mathbf{0} \\ \mathbf{0} & | & \tau \mathbf{I} \end{pmatrix}.$$

Obtaining a solution for this system is memory expensive and finding two suitable parameters  $\omega$  and  $\tau$  can be time consuming, since we can only choose them heuristically. However, the parameter reconstruction provides good results as shown in the next part.

**Numerical Realization.** We present a simple test model, where we consider a cube of a biological tissue with two inclusions (tumors) as depicted in Figure 1.

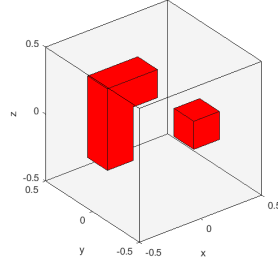


FIG. 1. Cube with two inclusions (red).

The Lamé parameters of the corresponding materials are given in Table 1.

material	$\lambda_i$	$\mu_i$
$i = 0$ : tissue	$6.6211 \cdot 10^5$	$6.6892 \cdot 10^3$
$i = 1$ : tumor	$2.3177 \cdot 10^6$	$2.3411 \cdot 10^4$

TABLE 1  
Lamé parameter of the test material in [Pa].

For our numerical experiments, we simulate the discrete measurements by solving

$$(3.7) \quad \left\{ \begin{array}{ll} \nabla \cdot (\lambda_0(\nabla \cdot u_0)I + 2\mu_0 \hat{\nabla} u_0) &= 0 \quad \text{in } \Omega, \\ -\nabla \cdot \left( ((\lambda_1 - \lambda_0)\chi_D)(\nabla \cdot u_0)I + 2((\mu_1 - \mu_0)\chi_D)\hat{\nabla} u_0 \right) \\ \quad + \nabla \cdot (\lambda(\nabla \cdot v)I + 2\mu \hat{\nabla} v) &= 0 \quad \text{in } \Omega, \\ (\lambda_0(\nabla \cdot u_0)I + 2\mu_0 \hat{\nabla} u_0)n &= g_l \quad \text{on } \Gamma_N, \\ (\lambda(\nabla \cdot v)I + 2\mu \hat{\nabla} v)n &= 0 \quad \text{on } \Gamma_N, \\ u_0 &= 0 \quad \text{on } \Gamma_D, \\ v &= 0 \quad \text{on } \Gamma_D, \end{array} \right.$$

for each of the  $l = 1, \dots, M$  given boundary forces  $g_l$ , where  $v := u_0 - u$  are the difference measurements. The equations regarding  $v$  in the system (3.7) result from subtracting the boundary value problem (2.1) for the respective Lamé parameters.

**Exact Data.** First of all, we take a look at the example without noise, which means we assume we are given exact data.

In order to obtain a suitable visualization of the 3D reconstruction, we manipulate the transparency parameter function  $\alpha : \mathbb{R} \rightarrow [0, 1]$  of Figure 3 as exemplary depicted for the Lamé parameter  $\mu$  in Figure 2. It should be noted that a low transparency parameter indicates that the corresponding color (here, the colors around zero) are plotted with high transparency, while a high  $\alpha$  indicates that the corresponding color is plotted opaque. The reason for this choice is that values of the calculated difference  $\kappa = \mu_1 - \mu_0$  close to zero are not an indication of an inclusion, while values with a higher absolute value indicate an inclusion. Hence, this choice of transparency is

suitable to plot the calculated inclusions without being covered by white tetrahedrons with values close to zero. Further, the reader should observe that  $\alpha(\kappa) > 0$  for all values of  $\kappa$ , so that all tetrahedrons are plotted and that the transparency plot for  $\nu$  takes the same shape but is adjusted to the range of the calculated values.

The following results (Figure 3 - Figure 4) are based on a parameter search and the regularization parameters are chosen heuristically. Thus, we only present the results with the best parameter choice ( $\omega = 10^{-17}$  and  $\tau = 10^{-13}$ ) and reconstruct the difference in the Lamé parameters  $\mu$  and  $\lambda$ .

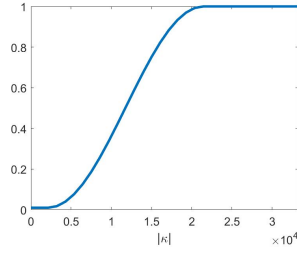


FIG. 2. Transparency function for the plots in Figure 3 mapping the values of  $\kappa$  to  $\alpha(\kappa)$ .

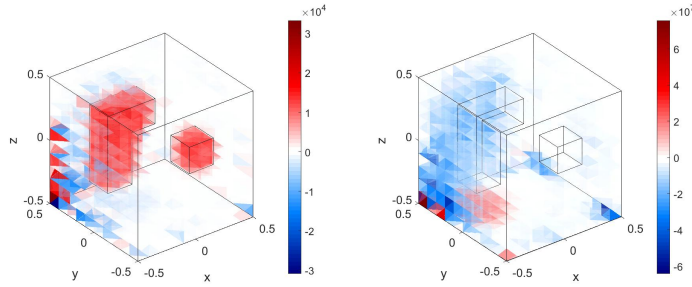


FIG. 3. Shape reconstruction of two inclusions of the difference in the Lamé parameter  $\mu$  (left hand side) and  $\lambda$  (right hand side) for the regularization parameters  $\omega = 10^{-17}$  and  $\tau = 10^{-13}$  without noise and transparency function  $\alpha$  as shown in Figure 2.

With these regularization parameters, the two inclusions are detected and reconstructed correctly for  $\mu$  (see Figure 3 in the left hand side) and the value of  $\mu - \mu_0$  is in the correct amplitude range as depicted in Figure 4. Figure 3 shows us, that for  $\lambda - \lambda_0$ , the reconstruction does not work. The reason is that the range of the Lamé parameters differs from each other around  $10^2$  Pa ( $\lambda \approx 100 \cdot \mu$ ), but

$$\|\mathbf{S}^\mu\|_2 \approx 1.2 \cdot 10^4 \|\mathbf{S}^\lambda\|_2,$$

i.e. the signatures of  $\mu$  are represented far stronger in the calculation of  $\mathbf{V}$  than those of  $\lambda$ .

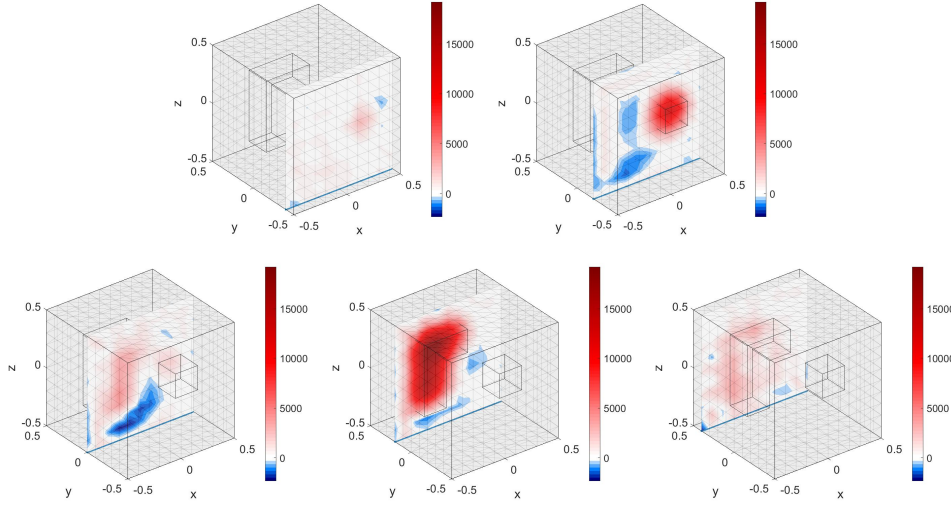


FIG. 4. Shape reconstruction of two inclusions of the reconstructed difference in the Lamé parameter  $\mu$  for the regularization parameters  $\omega = 10^{-17}$  and  $\tau = 10^{-13}$  depicted as cuts without noise.

**Noisy Data.** Next, we go over to noisy data. We assume that we are given a noise level  $\eta \geq 0$  and set

$$(3.8) \quad \delta = \eta \cdot \|\mathbf{\Lambda}(\lambda, \mu)\|_F.$$

Further, we define  $\mathbf{\Lambda}^\delta(\lambda, \mu)$  as

$$(3.9) \quad \mathbf{\Lambda}^\delta(\lambda, \mu) = \mathbf{\Lambda}(\lambda, \mu) + \delta \bar{\mathbf{E}},$$

with  $\bar{\mathbf{E}} = \mathbf{E}/\|\mathbf{E}\|_F$ , where  $\mathbf{E}$  consists of  $M \times M$  random values in  $[-1, 1]$ . Hence, we have

$$\|\mathbf{V}^\delta - \mathbf{V}\| \leq \delta.$$

In the following examples, we consider relative noise levels of  $\eta = 1\%$  (Figure 5) and  $\eta = 10\%$  (Figure 7 and 8) with respect to the Frobenius norm as given in (3.9), where the regularization parameters are chosen heuristically and given in the caption of the figure.

In Figure 5, we observe that for a low noise level with  $\eta = 1\%$ , we obtain a suitable reconstruction of the inclusion concerning the Lamé parameter  $\mu$  and the reconstruction of  $\lambda$  fails again.

In contrary to the low noise level ( $\eta = 1\%$ ), Figures 7 and 8 show us that the standard one-step linearization method has problems in handling higher noise levels ( $\eta = 10\%$ ). As such, in the 3D reconstruction (see Figure 7) it is hard to recognize the two inclusions even with respect to the Lamé parameter  $\mu$ . Further on in the plots of the cuts in Figure 8, the reconstructions of the inclusions are blurred out.



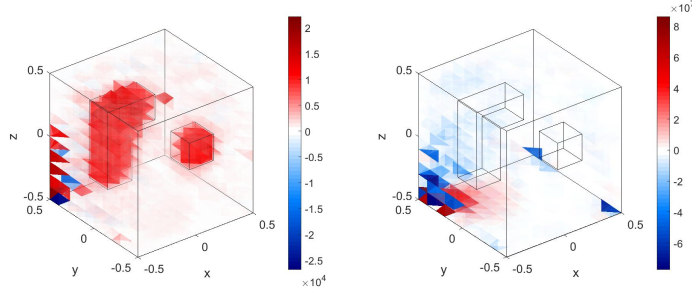


FIG. 5. Shape reconstruction of two inclusions of the difference in the Lamé parameter  $\mu$  (left hand side) and  $\lambda$  (right hand side) for the regularization parameters  $\omega = 1.1 \cdot 10^{-17}$  and  $\tau = 1.1 \cdot 10^{-13}$  with relative noise  $\eta = 1\%$  and transparency function  $\alpha$  as shown in Figure 2.

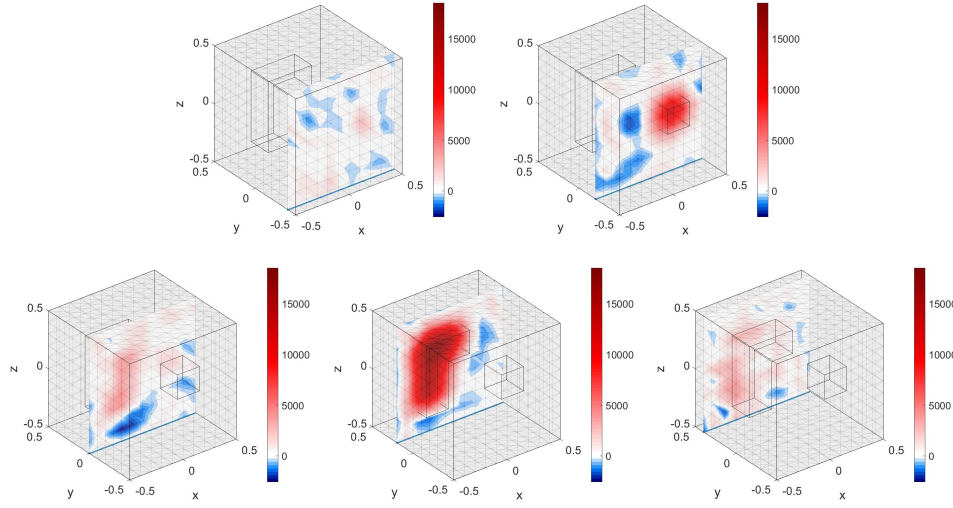


FIG. 6. Shape reconstruction of two inclusions of the reconstructed difference in the Lamé parameter  $\mu$  for the regularization parameters  $\omega = 1.1 \cdot 10^{-17}$  and  $\tau = 1.1 \cdot 10^{-13}$  depicted as cuts with relative noise  $\eta = 1\%$ .

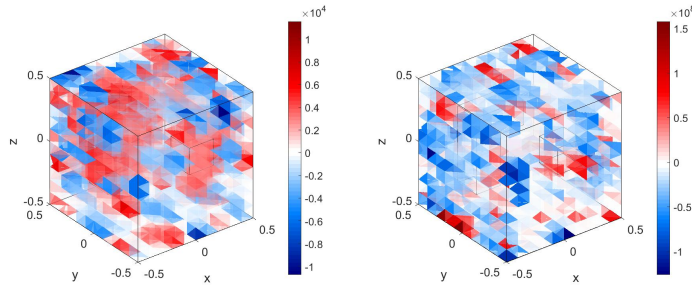


FIG. 7. Shape reconstruction of two inclusions of the difference in the Lamé parameter  $\mu$  (left hand side) and  $\lambda$  (right hand side) for the regularization parameters  $\omega = 6 \cdot 10^{-17}$  and  $\tau = 6 \cdot 10^{-13}$  with relative noise  $\eta = 10\%$  and transparency function  $\alpha$  as shown in Figure 2.

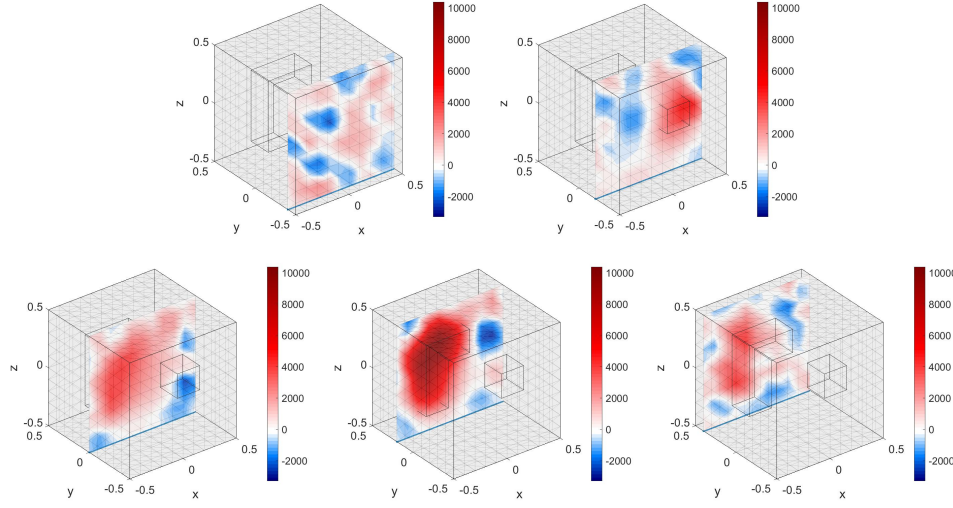


FIG. 8. Shape reconstruction of two inclusions of the reconstructed difference in the Lamé parameter  $\mu$  for the regularization parameters  $\omega = 6 \cdot 10^{-17}$  and  $\tau = 6 \cdot 10^{-13}$  depicted as cuts with relative noise  $\eta = 10\%$ .

*Remark 3.1.* All in all, the numerical experiments of this section motivate the consideration of a modified minimization problem in order to obtain a stable method for noisy data as well as a good reconstruction for the Lamé parameter  $\lambda$ . In doing so, we will combine the idea of the standard one-step linearization with the monotonicity method.

**4. Enhancing the Standard Residual-based Minimization Problem.** We summarize and present the required results concerning the monotonicity properties of the Neumann-to-Dirichlet operator as well as the monotonicity methods introduced and proven in [6] and [5].

**4.1. Summary of the Monotonicity Methods.** First, we state the monotonicity estimates for the Neumann-to-Dirichlet operator  $\Lambda(\lambda, \mu)$ .

LEMMA 4.1 (Lemma 3.1 from [6]). *Let  $(\lambda_0, \mu_0), (\lambda_1, \mu_1) \in L_+^\infty(\Omega) \times L_+^\infty(\Omega)$ ,  $g \in L^2(\Gamma_N)^d$  be an applied boundary force, and let  $u_0 := u_{(\lambda_0, \mu_0)}^g \in \mathcal{V}$ ,  $u_1 := u_{(\lambda_1, \mu_1)}^g \in \mathcal{V}$ . Then*

$$(4.1) \quad \begin{aligned} & \int_{\Omega} 2(\mu_0 - \mu_1) \hat{\nabla} u_1 : \hat{\nabla} u_1 + (\lambda_0 - \lambda_1) \nabla \cdot u_1 \nabla \cdot u_1 \, dx \\ & \geq \langle g, \Lambda(\lambda_1, \mu_1) g \rangle - \langle g, \Lambda(\lambda_0, \mu_0) g \rangle \end{aligned}$$

$$(4.2) \quad \geq \int_{\Omega} 2(\mu_0 - \mu_1) \hat{\nabla} u_0 : \hat{\nabla} u_0 + (\lambda_0 - \lambda_1) \nabla \cdot u_0 \nabla \cdot u_0 \, dx.$$

LEMMA 4.2 (Lemma 2 from [5]). *Let  $(\lambda_0, \mu_0), (\lambda_1, \mu_1) \in L_+^\infty(\Omega) \times L_+^\infty(\Omega)$ ,  $g \in L^2(\Gamma_N)^d$  be an applied boundary force, and let  $u_0 := u_{(\lambda_0, \mu_0)}^g \in \mathcal{V}$ ,  $u_1 := u_{(\lambda_1, \mu_1)}^g \in \mathcal{V}$ .*

Then

$$\begin{aligned}
 (4.3) \quad & \langle g, \Lambda(\lambda_1, \mu_1)g \rangle - \langle g, \Lambda(\lambda_0, \mu_0)g \rangle \\
 & \geq \int_{\Omega} 2 \left( \mu_1 - \frac{\mu_1^2}{\mu_0} \right) \hat{\nabla} u_1 : \hat{\nabla} u_1 \, dx + \int_{\Omega} \left( \lambda_1 - \frac{\lambda_1^2}{\lambda_0} \right) \nabla \cdot u_1 \nabla \cdot u_1 \, dx \\
 (4.4) \quad & = \int_{\Omega} 2 \frac{\mu_1}{\mu_0} (\mu_0 - \mu_1) \hat{\nabla} u_1 : \hat{\nabla} u_1 \, dx + \int_{\Omega} \frac{\lambda_1}{\lambda_0} (\lambda_0 - \lambda_1) \nabla \cdot u_1 \nabla \cdot u_1 \, dx.
 \end{aligned}$$

COROLLARY 4.3 (Corollary 3.2 from [6]). For  $(\lambda_0, \mu_0), (\lambda_1, \mu_1) \in L_+^\infty(\Omega) \times L_+^\infty(\Omega)$

$$(4.5) \quad \lambda_0 \leq \lambda_1 \text{ and } \mu_0 \leq \mu_1 \quad \text{implies} \quad \Lambda(\lambda_0, \mu_0) \geq \Lambda(\lambda_1, \mu_1).$$

Further on, we give a short overview concerning the monotonicity methods, where we restrict ourselves to the case  $\lambda_1 \geq \lambda_0$ ,  $\mu_1 \geq \mu_0$ . In the following, let  $\mathcal{D}$  be the unknown inclusion and  $\chi_{\mathcal{D}}$  the characteristic function w.r.t.  $\mathcal{D}$ .

COROLLARY 4.4. *Linearized monotonicity test (Corollary 2.7 from [5])*  
 Let  $\lambda_0, \lambda_1, \mu_0, \mu_1 \in \mathbb{R}^+$  with  $\lambda_1 > \lambda_0$ ,  $\mu_1 > \mu_0$  and assume that  $(\lambda, \mu) = (\lambda_0 + (\lambda_1 - \lambda_0)\chi_{\mathcal{D}}, \mu_0 + (\mu_1 - \mu_0)\chi_{\mathcal{D}})$  with  $\mathcal{D} = \text{out}_{\partial\Omega} \text{supp}((\lambda - \lambda_0, \mu - \mu_0)^T)$ . Further on let  $\alpha^\lambda, \alpha^\mu \geq 0$ ,  $\alpha^\lambda + \alpha^\mu > 0$  and  $\alpha^\lambda \leq \frac{\lambda_0}{\lambda_1}(\lambda_1 - \lambda_0)$ ,  $\alpha^\mu \leq \frac{\mu_0}{\mu_1}(\mu_1 - \mu_0)$ . Then for every open set  $\mathcal{B}$

$$\mathcal{B} \subseteq \mathcal{D} \quad \text{if and only if} \quad \Lambda(\lambda_0, \mu_0) + \Lambda'(\lambda_0, \mu_0)(\alpha^\lambda \chi_{\mathcal{B}}, \alpha^\mu \chi_{\mathcal{B}}) \geq \Lambda(\lambda, \mu).$$

COROLLARY 4.5. *Linearized monotonicity test for noisy data (Corollary 2.9 from [5])*

Let  $\lambda_0, \lambda_1, \mu_0, \mu_1 \in \mathbb{R}^+$  with  $\lambda_1 > \lambda_0$ ,  $\mu_1 > \mu_0$  and assume that  $(\lambda, \mu) = (\lambda_0 + (\lambda_1 - \lambda_0)\chi_{\mathcal{D}}, \mu_0 + (\mu_1 - \mu_0)\chi_{\mathcal{D}})$  with  $\mathcal{D} = \text{out}_{\partial\Omega} \text{supp}((\lambda - \lambda_0, \mu - \mu_0)^T)$ . Further on, let  $\alpha^\lambda, \alpha^\mu \geq 0$ ,  $\alpha^\lambda + \alpha^\mu > 0$  with  $\alpha^\lambda \leq \frac{\lambda_0}{\lambda_1}(\lambda_1 - \lambda_0)$ ,  $\alpha^\mu \leq \frac{\mu_0}{\mu_1}(\mu_1 - \mu_0)$ . Let  $\Lambda^\delta$  be the Neumann-to-Dirichlet operator for noisy difference measurements with noise level  $\delta > 0$ . Then for every open set  $\mathcal{B} \subseteq \Omega$  there exists a noise level  $\delta_0 > 0$ , such that for all  $0 < \delta < \delta_0$ ,  $\mathcal{B}$  is correctly detected as inside or not inside the inclusion  $\mathcal{D}$  by the following monotonicity test

$$\mathcal{B} \subseteq \mathcal{D} \quad \text{if and only if} \quad \Lambda(\lambda_0, \mu_0) + \Lambda'(\lambda_0, \mu_0)(\alpha^\lambda \chi_{\mathcal{B}}, \alpha^\mu \chi_{\mathcal{B}}) - \Lambda^\delta(\lambda, \mu) + \delta I \geq 0.$$

Finally, we present the result (see Figure 9) obtained from noisy data  $\Lambda^\delta$  with the linearized monotonicity method as described in Corollary 4.5, where we use the same pixel partition as for the one-step linearization method.

*Remark 4.6.* The linearized monotonicity method converges theoretically rigorously, but in practice delivers poorer reconstructions even for small noise (see Figure 9, where the two inclusions are not separated) than the theoretically unproven heuristic one-step linearization (see Figure 5, where the two inclusions are separated). Thus, we improve the standard one-step linearization method by combining it with the monotonicity method without losing the convergence results.

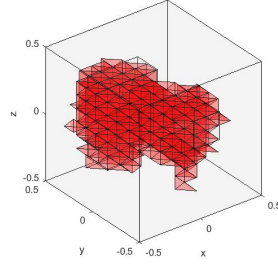


FIG. 9. Shape reconstruction of two inclusions (red) for  $\alpha^\lambda = 0.28(\lambda_1 - \lambda_0) \approx 4.6 \cdot 10^5 Pa$ ,  $\alpha^\mu = 0.28(\mu_1 - \mu_0) \approx 4.7 \cdot 10^3 Pa$  with relative noise  $\eta = 0.1\%$  and  $\delta = 1.88 \cdot 10^{-10}$ .

**4.2. Monotonicity-based Regularization.** For the following, we assume again that the background  $(\lambda_0, \mu_0)$  is homogeneous and that the contrasts of the anomalies  $(\gamma^\lambda, \gamma^\mu)^T \in L_+^\infty(\mathcal{D})^2$  with

$$\begin{pmatrix} \lambda(x) \\ \mu(x) \end{pmatrix} = \begin{pmatrix} \lambda_0 + \gamma^\lambda(x)\chi_{\mathcal{D}}(x) \\ \mu_0 + \gamma^\mu(x)\chi_{\mathcal{D}}(x) \end{pmatrix},$$

are bounded for all  $x \in \mathcal{D}$  (a.e.) via

$$c^\lambda \leq \gamma^\lambda(x) \leq C^\lambda \quad \text{and} \quad c^\mu \leq \gamma^\mu(x) \leq C^\mu,$$

with  $c^\lambda, C^\lambda, c^\mu, C^\mu \geq 0$ .  $\mathcal{D}$  is an open set denoting the anomalies and the parameters  $\lambda_0, \mu_0, c^\lambda, c^\mu, C^\lambda$  and  $C^\mu$  are assumed to be known.

Here, we focus on the case  $\lambda \geq \lambda_0$ ,  $\mu \geq \mu_0$ , while the case  $\lambda \leq \lambda_0$ ,  $\mu \leq \mu_0$  can be found in the Appendix.

Similar as in the one-step linearization method, we make the piecewise constant ansatz (3.1) in order to approximate  $(\gamma^\lambda, \gamma^\mu)$  by  $(\kappa, \nu)$ .

The main idea of monotonicity-based regularization is to minimize the residual of the linearized problem, i.e.,

$$(4.6) \quad \left\| (\mathbf{S}^\lambda \mid \mathbf{S}^\mu) \begin{pmatrix} \kappa \\ \nu \end{pmatrix} - \mathbf{V} \right\|_2^2 \rightarrow \min!$$

with constraints on  $(\kappa, \nu)$  that are obtained from the monotonicity properties introduced in Lemma 4.1 and 4.2. Our aim is to rewrite the minimization problem (4.6) for the case  $\mu_0 \neq \mu$ ,  $\lambda_0 \neq \lambda$  in  $\mathcal{D}$  in order to be able to reconstruct the inclusions also with respect to  $\lambda$ . Our intention is to force that both Lamé parameters  $\mu(x)$  and  $\lambda(x)$  take the same shape but different scale.

In more detail, we define the quantities  $a_{\max}$  and  $\tau$  as

$$(4.7) \quad a_{\max} := \mu_0 - \frac{\mu_0^2}{\mu_0 + c^\mu},$$

$$(4.8) \quad \tau := \frac{1}{a_{\max}} \left( \lambda_0 - \frac{\lambda_0^2}{\lambda_0 + c^\lambda} \right),$$

such that

$$(4.9) \quad -2 \left( \mu_0 - \frac{\mu_0^2}{\mu} \right) + 2a \leq 0,$$

$$(4.10) \quad - \left( \lambda_0 - \frac{\lambda_0^2}{\lambda} \right) + \tau a \leq 0$$

for all  $0 \leq a \leq a_{\max}$ .

In addition, we set the residual  $r(\nu)$  as

$$r(\nu) := \Lambda(\lambda, \mu) - \Lambda(\lambda_0, \mu_0) - \Lambda'(\lambda_0, \mu_0)(\tau\nu, \nu)$$

and the components of the corresponding matrix  $\mathbf{R}(\nu)$  are given by

$$(\mathbf{R}(\nu))_{i,j=1,\dots,M} := (\langle g_i, r(\nu)g_j \rangle)_{i,j=1,\dots,M}.$$

Finally, we introduce the set

$$\mathcal{C} := \left\{ \nu \in L_+^\infty(\Omega) : \nu = \sum_{k=1}^p a_k \chi_k, a_k \in \mathbb{R}, 0 \leq a_k \leq \min(a_{\max}, \beta_k) \right\}$$

with

$$(4.11) \quad \beta_k := \max \{a \geq 0 : \Lambda(\lambda, \mu) - \Lambda(\lambda_0, \mu_0) \leq \Lambda'(\lambda_0, \mu_0)(\tau a \chi_k, a \chi_k)\},$$

where we denote by  $\chi_k := \chi_{\mathcal{B}_k}$ .

Then, we modify the original minimization problem (4.6) to

$$\min_{\nu \in \mathcal{C}} \|\mathbf{R}(\nu)\|_F.$$

*Remark 4.7.* We want to remark that  $\beta_k$  is defined via the infinite-dimensional Neumann-to-Dirichlet operator  $\Lambda(\lambda, \mu)$  and does not involve the finite dimensional matrix  $\mathbf{R}$ . For the numerical realization we will require a discrete version  $\tilde{\beta}_k$  of  $\beta_k$  introduced later on.

**4.2.1. Main Results.** In the following we present our main results and will show that the choices of the quantities  $a_{\max}$  and  $\tau$  will lead the correct reconstruction of the support of  $\mu(x)$  and  $\nu(x)$ , which we introduced in (4.7) and (4.8), respectively, based on the lower bounds from the monotonicity tests as stated in (4.9) and (4.10).

**THEOREM 4.8.** *Consider the minimization problem*

$$(4.12) \quad \min_{\nu \in \mathcal{C}} \|\mathbf{R}(\nu)\|_F.$$

*The following statements hold true:*

- (i) *Problem (4.12) admits a unique minimizer  $\hat{\nu}$ .*
- (ii)  *$\text{supp}(\hat{\nu})$  and  $\mathcal{D}$  agree up to the pixel partition, i.e. for any pixel  $\mathcal{B}_k$*

$$\mathcal{B}_k \subset \text{supp}(\hat{\nu}) \quad \text{if and only if} \quad \mathcal{B}_k \subset \mathcal{D}.$$

*Moreover,*

$$\hat{\nu} = \sum_{\mathcal{B}_k \subseteq \mathcal{D}} a_{\max} \chi_k.$$

Now we deal with noisy data and introduce the corresponding residual

$$r_\delta(\nu) := \Lambda^\delta(\lambda, \mu) - \Lambda(\lambda_0, \mu_0) - \Lambda'(\lambda_0, \mu_0)(\tau\nu, \nu).$$

Based on this,  $\mathbf{R}_\delta(\nu)$  represents the matrix  $(\langle g_i, r_\delta(\nu)g_j \rangle)_{i,j=1,\dots,M}$ .

Further on, the admissible set for noisy data is defined by

$$\mathcal{C}_\delta := \left\{ \nu \in L_+^\infty(\Omega) : \nu = \sum_{k=1}^p a_k \chi_k, a_k \in \mathbb{R}, 0 \leq a_k \leq \min(a_{\max}, \beta_{k,\delta}) \right\}$$

with

$$(4.13) \quad \beta_{k,\delta} := \max \{ a \geq 0 : \Lambda^\delta(\lambda, \mu) - \Lambda(\lambda_0, \mu_0) - \delta I \leq \Lambda'(\lambda_0, \mu_0)(\tau a \chi_k, a \chi_k) \}.$$

Thus, we present the following stability result.

**THEOREM 4.9.** *Consider the minimization problem*

$$(4.14) \quad \min_{\nu \in \mathcal{C}_\delta} \|\mathbf{R}_\delta(\nu)\|_F.$$

The following statements hold true:

- (i) Problem (4.14) admits a minimizer.
- (ii) Let  $\hat{\nu} = \sum_{\mathcal{B}_k \subseteq \mathcal{D}} a_{\max} \chi_k$  be the minimizer (4.12) and  $\hat{\nu}_\delta = \sum_{k=1}^p a_{k,\delta} \chi_k$  of problem (4.14), respectively. Then  $\hat{\nu}_\delta$  converges pointwise and uniformly to  $\hat{\nu}$  as  $\delta$  goes to 0.

**4.2.2. Theoretical Background.** In order to prove Theorem 4.8 as well as Theorem 4.9, we have to take a look at the following.

**LEMMA 4.10.** *Let  $a_{\max}$  and  $\tau$  and be defined as in (4.9) and (4.10), respectively,  $\lambda, \mu \in L_+^\infty(\Omega)$  and we assume that  $\lambda \geq \lambda_0$ ,  $\mu \geq \mu_0$ , where  $\lambda_0, \mu_0$  are constant. Then we have for any pixel  $\mathcal{B}_k$ ,  $\mathcal{B}_k \subseteq \mathcal{D}$  if and only if  $\beta_k > 0$ , where  $\beta_k$  is defined in (4.11).*

*Proof.* We adopt the proof of Lemma 3.4 from [9].

*Step 1:* We shall check that  $\mathcal{B}_k \subseteq \mathcal{D}$  implies  $\beta_k > 0$ .

Indeed, applying the monotonicity principle (4.3) for

$$\lambda_1 := \lambda \text{ and } \mu_1 := \mu,$$

we get the following inequalities for all pixel  $\mathcal{B}_k$ , all  $a \in [0, a_{\max}]$  and all  $g \in L^2(\Gamma_N)^d$

$$\begin{aligned} & \langle g, (\Lambda(\lambda, \mu) - \Lambda(\lambda_0, \mu_0) - \Lambda'(\lambda_0, \mu_0)(\tau a \chi_k, a \chi_k)) g \rangle \\ & \leq - \int_{\Omega} 2 \left( \mu_0 - \frac{\mu_0^2}{\mu} \right) \hat{\nabla} u_0^g : \hat{\nabla} u_0^g + 2a \chi_k \hat{\nabla} u_0^g : \hat{\nabla} u_0^g dx \\ & \quad - \int_{\Omega} \left( \lambda_0 - \frac{\lambda_0^2}{\lambda} \right) \nabla \cdot u_0^g \nabla \cdot u_0^g dx + \tau a \chi_k \nabla \cdot u_0^g \nabla \cdot u_0^g dx \\ & \leq - \int_{\mathcal{D}} 2 \left( \mu_0 - \frac{\mu_0^2}{\mu} \right) \hat{\nabla} u_0^g : \hat{\nabla} u_0^g dx + \int_{\mathcal{B}_k} 2a_{\max} \hat{\nabla} u_0^g : \hat{\nabla} u_0^g dx \\ & \quad - \int_{\mathcal{D}} \left( \lambda_0 - \frac{\lambda_0^2}{\lambda} \right) \nabla \cdot u_0^g \nabla \cdot u_0^g dx + \int_{\mathcal{B}_k} \tau a_{\max} \nabla \cdot u_0^g \nabla \cdot u_0^g dx \\ & \leq 0. \end{aligned}$$

Here,  $u_0^g$  is the unique solution of the forward problem when the background Lamé parameter is chosen to be  $\lambda_0, \mu_0$ . The last inequality holds due to the fact that  $a_{\max}$  and  $\tau$  fulfill

$$\begin{aligned} -2 \left( \mu_0 - \frac{\mu_0^2}{\mu} \right) + 2a_{\max} &\leq 0, \\ - \left( \lambda_0 - \frac{\lambda_0^2}{\lambda} \right) + \tau a_{\max} &\leq 0 \end{aligned}$$

in  $\mathcal{D}$  and that  $\mathcal{B}_k$  lies inside  $\mathcal{D}$ .

*Step 2:* If  $\beta_k > 0$ , we will show that  $\mathcal{B}_k \subseteq \mathcal{D}$  by contradiction.

Assume that  $\mathcal{B}_k \not\subseteq \mathcal{D}$  and  $\beta_k > 0$ . Applying the monotonicity principle from Lemma 4.1,

$$\Lambda(\lambda, \mu) - \Lambda(\lambda_0, \mu_0) \geq \Lambda'(\lambda_0, \mu_0)((\lambda, \mu) - (\lambda_0, \mu_0)),$$

we get for all  $g \in L^2(\Gamma_N)^d$

$$\begin{aligned} (4.15) \quad & \int_{\mathcal{B}_k} \tau \beta_k \nabla \cdot u_0^g \nabla \cdot u_0^g dx + 2 \int_{\mathcal{B}_k} \beta_k \hat{\nabla} u_0^g : \hat{\nabla} u_0^g dx \\ & \leq \int_{\Omega} (\lambda - \lambda_0) \nabla \cdot u_0^g \nabla \cdot u_0^g dx + 2 \int_{\Omega} (\mu - \mu_0) \hat{\nabla} u_0^g : \hat{\nabla} u_0^g dx \\ & \leq \int_{\mathcal{D}} C^\lambda \nabla \cdot u_0^g \nabla \cdot u_0^g dx + 2 \int_{\mathcal{D}} C^\mu \hat{\nabla} u_0^g : \hat{\nabla} u_0^g dx. \end{aligned}$$

On the other hand, applying the localized potentials in a similar procedure as in the proof of Theorem 2.1 in [5], we can find a sequence  $(g_m)_{m \in \mathbb{N}} \subset L^2(\Gamma_N)^d$  such that the solutions  $(u_0^m)_{m \in \mathbb{N}} \subset H^1(\Omega)^d$  of the forward problem (when the Lamé parameter are chosen to be  $\lambda_0, \mu_0$  and the boundary forces  $g = g_m$ ) fulfill

$$\begin{aligned} \lim_{m \rightarrow \infty} \int_{\mathcal{B}_k} \hat{\nabla} u_0^m : \hat{\nabla} u_0^m dx &= \infty, & \lim_{m \rightarrow \infty} \int_{\mathcal{D}} \hat{\nabla} u_0^m : \hat{\nabla} u_0^m dx &= 0, \\ \lim_{m \rightarrow \infty} \int_{\mathcal{B}_k} \nabla \cdot u_0^m \nabla \cdot u_0^m dx &= \infty, & \lim_{m \rightarrow \infty} \int_{\mathcal{D}} \nabla \cdot u_0^m \nabla \cdot u_0^m dx &= 0, \end{aligned}$$

which contradicts (4.15).  $\square$

LEMMA 4.11. For all pixels  $\mathcal{B}_k$ , denote by  $\mathbf{S}_k^\tau$  the matrix

$$\mathbf{S}_k^\tau := (\langle g_i, -(\mathbf{S}^\mu + \tau \mathbf{S}^\lambda)_{i,j} g_j \rangle)_{i,j=1,\dots,M}.$$

Then  $\mathbf{S}_k^\tau$  is a positive definite matrix.

*Proof.* We adopt the proof of Lemma 3.5 from [9] for the matrix  $\mathbf{S}_k^\tau$ , which directly yields the desired result.  $\square$

*Proof. (Theorem 4.8)* This proof is based on the proof of Theorem 3.2 from [9].  
to (i) Since the functional

$$\nu \mapsto \|\mathbf{R}(\nu)\|_F^2 := \sum_{i,j=1}^M \langle g_i, r(\nu)g_j \rangle^2$$

is continuous, it admits a minimizer in the compact set  $\mathcal{C}$ .  
The uniqueness of  $\hat{\nu}$  will follow from the proof of (ii) *Step 3*.

to (ii) *Step 1* We shall check that for all

$$\nu = \sum_{k=1}^p a_k \chi_k \quad \text{satisfying} \quad 0 \leq a_k \leq \min(a_{\max}, \beta_k),$$

it holds that  $r(\nu) \leq 0$  in quadratic sense. We want to remark that for  $a_{\max}$  and  $\tau$  it holds that (4.9) and (4.10) in  $\mathcal{D}$ .

In the same manner as in the proof of Lemma 4.10, we can write

$$\begin{aligned} & \langle g, (\Lambda(\lambda, \mu) - \Lambda(\lambda_0, \mu_0) - \Lambda'(\lambda_0, \mu_0)(\tau\nu, \nu))g \rangle \\ & \leq - \int_{\mathcal{D}} a_{\max} \hat{\nabla} u_0^g : \hat{\nabla} u_0^g dx + \sum_{k=1}^p \int_{\mathcal{B}_k} a_k \hat{\nabla} u_0^g : \hat{\nabla} u_0^g dx \\ & \quad - \int_{\mathcal{D}} \tau a_{\max} \nabla \cdot u_0^g \nabla \cdot u_0^g dx + \sum_{k=1}^p \int_{\mathcal{B}_k} \tau a_k \nabla \cdot u_0^g \nabla \cdot u_0^g dx \end{aligned}$$

for any  $g \in L^2(\Gamma_N)^d$ .

If  $a_k > 0$ , we have  $\beta_k \geq a_k > 0$ , so that by Lemma 4.10, it holds that  $\mathcal{B}_k \subseteq \mathcal{D}$ . Taking into account that  $a_k \leq a_{\max}$ , we get that  $\langle g, r(\nu)g \rangle \leq 0$  for  $g \in L^2(\Gamma_N)^d$ .

*Step 2:* Let  $\hat{\nu} = \sum_{k=1}^p \hat{a}_k \chi_k$  be a minimizer of problem (4.12). We prove that  $\text{supp}(\hat{\nu}) \subseteq \mathcal{D}$ .

Per definition of  $\beta_k$ , it holds that  $\beta_k \geq \hat{a}_k$ . This implies  $\beta_k > 0$ . With Lemma 4.10 we have  $\mathcal{B}_k \subseteq \mathcal{D}$ .

*Step 3:*

We will show that, if  $\hat{\nu} = \sum_{k=1}^p \hat{a}_k \chi_k$  is a minimizer of problem (4.12), then the representation of  $\hat{a}_k$  is given by

$$\hat{a}_k = \begin{cases} 0 & \text{for } \mathcal{B}_k \not\subseteq \mathcal{D}, \\ a_{\max} & \text{for } \mathcal{B}_k \subseteq \mathcal{D}. \end{cases}$$

Indeed, it holds that  $\hat{a}_k < a_{\max}$ . If there exists a pixel  $\mathcal{B}_k$  such that  $\hat{\nu}(x) < \min(a_{\max}, \beta_k)$  in  $\mathcal{B}_k$ , we can choose  $h^\nu > 0$ , such that  $\hat{\nu} + h^\nu \chi_k = a_{\max}$  in  $\mathcal{B}_k$ . We will show that then,

$$\|\mathbf{R}(\hat{\nu} + h^\nu \chi_k)\|_F < \|\mathbf{R}(\hat{\nu})\|_F,$$

which contradicts the minimality of  $\hat{\nu}$ . Thus, it follows that  $\hat{a}_k = \min(a_{\max}, \beta_k)$ .



To show the contradiction, let  $\theta_1(\hat{\nu}) \geq \theta_2(\hat{\nu}) \geq \dots \geq \theta_M(\hat{\nu})$  be  $M$  eigenvalues of  $\mathbf{R}(\hat{\nu})$  and  $\theta_1(\hat{\nu} + h^\nu \chi_k) \geq \theta_2(\hat{\nu} + h^\nu \chi_k) \geq \dots \geq \theta_M(\hat{\nu} + h^\nu \chi_k)$   $M$  eigenvalues of  $\mathbf{R}(\hat{\nu} + h^\nu \chi_k)$ .

Since  $\mathbf{R}(\hat{\nu})$  and  $\mathbf{R}(\hat{\nu} + h^\nu \chi_k)$  are both symmetric, all of their eigenvalues are real. By the definition of the Frobenius norm, we get

$$\begin{aligned} & \|\mathbf{R}(\hat{\nu} + h^\nu \chi_k)\|_F^2 - \|\mathbf{R}(\hat{\nu})\|_F^2 \\ &= \sum_{i=1}^M |\theta_i(\hat{\nu} + h^\nu)|^2 - \sum_{i=1}^M |\theta_i(\hat{\nu})|^2 \\ &= \sum_{i=1}^M (\theta_i(\hat{\nu} + h^\nu \chi_k) + \theta_i(\hat{\nu})) \cdot (\theta_i(\hat{\nu} + h^\nu \chi_k) - \theta_i(\hat{\nu})). \end{aligned}$$

Due to *Step 1*,  $r(\hat{\nu}) \leq 0$  and  $r(\hat{\nu} + h^\nu \chi_k) \leq 0$  in the quadratic sense. Thus, for all  $x = (x_1, \dots, x_M)^T \in \mathbb{R}^M$ , we have

$$x^T \mathbf{R}(\hat{\nu}) x = \sum_{i,j=1}^M x_i x_j \langle g_i, r(\hat{\nu}) g_j \rangle = \langle g, r(\hat{\nu}) g \rangle \leq 0,$$

where  $g = \sum_{i=1}^M x_i g_i$ . This means that  $-\mathbf{R}(\hat{\nu})$  is a positive semi-definite symmetric matrix in  $\mathbb{R}^{M \times M}$ . It is well-known that all eigenvalues of a positive semi-definite symmetric matrix should be non-negative. Thus,  $\theta_i(\hat{\nu}) \leq 0$  for all  $i \in \{1, \dots, M\}$ . In the same manner,  $-\mathbf{R}(\hat{\nu} + h^\nu \chi_k)$  is also a positive semi-definite matrix.

We want to remark, that  $\mathbf{S}_k^\tau$  is positive definite as proven in Lemma 4.11 and hence, all  $M$  eigenvalues of  $\theta_1(\mathbf{S}_k^\tau) \geq \dots \geq \theta_M(\mathbf{S}_k^\tau)$  are positive. Since

$$\mathbf{R}(\hat{\nu} + h^\nu \chi_k) = \mathbf{R}(\hat{\nu}) + h^\nu \mathbf{S}_k^\tau$$

and the matrices  $\mathbf{R}(\hat{\nu} + h^\nu \chi_k)$ ,  $\mathbf{R}(\hat{\nu}) + h^\nu$  and  $\mathbf{S}_k^\tau$  are symmetric, we can apply Weyl's Inequalities to get

$$\theta_i(\hat{\nu} + h^\nu \chi_k) \geq \theta_i(\hat{\nu}) + \theta_M(h^\nu \mathbf{S}_k^\tau) > \theta_i(\hat{\nu})$$

for all  $i \in \{1, \dots, M\}$ .

In summary we end up with

$$\|\mathbf{R}(\hat{\nu} + h^\nu \chi_k)\|_F < \|\mathbf{R}(\hat{\nu})\|_F,$$

which contradicts the minimality of  $\hat{\nu}$  and thus, ends the proof of *Step 3*.

*Step 4:* If  $\mathcal{B}_k \subseteq \mathcal{D}$ , then  $\mathcal{B}_k \subseteq \text{supp}(\hat{\nu})$ . Indeed, since  $\hat{\nu}$  is a minimizer of problem (4.12), *Step 3* implies that

$$\hat{\nu} = \sum_{k=1}^p \min(a_{\max}, \beta_k) \chi_k.$$

Since  $\mathcal{B}_k \subseteq \mathcal{D}$ , it follows from Lemma 4.10 that  $\min(a_{\max}, \beta_k) > 0$ . Thus,  $\mathcal{B}_k \subseteq \text{supp}(\hat{\nu})$ .

In conclusion, problem (4.12) admits a unique minimizer  $\hat{\nu}$  with

$$\hat{\nu} = \sum_{k=1}^p \min(a_{\max}, \beta_k) \chi_k.$$

This minimizer fulfills

$$\hat{\nu} = \begin{cases} a_{\max} & \text{in } \mathcal{B}_k, & \text{if } \mathcal{B}_k \text{ lies inside } \mathcal{D}, \\ 0 & \text{in } \mathcal{B}_k, & \text{if } \mathcal{B}_k \text{ does not lie inside } \mathcal{D}, \end{cases}$$

so that

$$\hat{\nu} = \sum_{\mathcal{B}_k \subseteq \mathcal{D}} a_{\max} \chi_k.$$

□

Next, we go over to noisy data and take a look at the following lemma.

**LEMMA 4.12.** *Assume that  $\|\Lambda^\delta(\lambda, \mu) - \Lambda(\lambda, \mu)\| \leq \delta$ . Then for every pixel  $\mathcal{B}_k$ , it holds that  $\beta_k \leq \beta_{k,\delta}$  for all  $\delta > 0$ .*

*Proof.* The proof follows the lines of Lemma 3.7 in [9] with the following modifications. We have to check that  $\beta_k$  fulfills the relation

$$|V^\delta| + \Lambda'(\lambda_0, \mu_0)(\tau a \chi_k, a \chi_k) \geq -\delta I \quad \text{for all } a \in [0, \beta_k].$$

As proven in [9], the operator  $V - V^\delta \geq -\delta I$  in quadratic sense. Further on Lemma 3.6 from [9] implies  $|V^\delta| \geq V^\delta$ . Hence,

$$\begin{aligned} & |V^\delta| + \Lambda'(\lambda_0, \mu_0)(\tau \beta_k \chi_k, \beta_k \chi_k) \\ & \geq V^\delta + \Lambda'(\lambda_0, \mu_0)(\tau \beta_k \chi_k, \beta_k \chi_k) \\ & = V + \Lambda'(\lambda_0, \mu_0)(\tau \beta_k \chi_k, \beta_k \chi_k) + V^\delta - V \\ & \geq -\delta I. \end{aligned}$$

□

**Remark 4.13.** As a consequence, it holds that

1. If  $\mathcal{B}_k$  lies inside  $\mathcal{D}$ , then  $\beta_{k,\delta} \geq a_{\max}$ .
2. If  $\beta_{k,\delta} = 0$ , then  $\mathcal{B}_k$  does not lie inside  $\mathcal{D}$ .

*Proof. (Theorem 4.9)* This proof is based on [9].

to (i) For the proof of the existence of a minimizer of (4.14), we argue as in the proof of Theorem 4.8 (i). Since the functional

$$\nu \mapsto \|\mathbf{R}_\delta(\nu)\|_F^2$$

is continuous, it follows that there exists at least one minimizer in the compact set  $\mathcal{C}^\delta$ .

to (ii) *Step 1:* Convergence of a subsequence of  $\hat{\nu}_\delta$

For any fixed  $k$ , the sequence  $\{\hat{a}_{k,\delta}\}_{\delta>0}$  is bounded from below by 0 and from above by  $a_{\max}$ , respectively. By Weierstrass' Theorem, there exists a subsequence  $(\hat{a}_{1,\delta_n}, \dots, \hat{a}_{p,\delta_n})$  converging to some limit  $(a_1, \dots, a_p)$ . Of course,  $0 \leq a_k \leq a_{\max}$  for all  $k = 1, \dots, p$ .

*Step 2: Upper bound and limit*

We shall check that  $a_k \leq \beta_k$  for all  $k = 1, \dots, p$ . As shown in the proof of Theorem 3.8 in [9],  $|V^\delta|$  converges to  $|V|$  and hence, for any fixed  $k$ ,

$$|V| + \Lambda'(\lambda_0, \mu_0)(\tau a_k \chi_k, a_k \chi_k) = \lim_{\delta_n \rightarrow 0} (|V^{\delta_n}| + \Lambda'(\lambda_0, \mu_0)(\tau \hat{a}_{k,\delta_n} \chi_k, \hat{a}_{k,\delta_n} \chi_k))$$

in the operator norm. As in [9], we end up with

$$\langle g, (|V| + \Lambda'(\lambda_0, \mu_0)(\tau a_k \chi_k, a_k \chi_k))g \rangle \geq 0.$$

*Step 3: Minimality of the limit*

By Lemma 4.12,  $\min(a_{\max}, \beta_k) \leq \min(a_{\max}, \beta_{k,\delta})$  for all  $k = 1, \dots, p$ . Thus,  $\hat{\nu}$  belongs to the admissible set  $\mathcal{C}_\delta$  of the minimization problem (4.14) for all  $\delta > 0$ . By minimality of  $\hat{\nu}_\delta$ , we obtain

$$\|\mathbf{R}_\delta(\hat{\nu}_\delta)\|_F \leq \|\mathbf{R}_\delta(\hat{\nu})\|_F.$$

Denote by  $\nu = \sum_{k=1}^p a_k \chi_k$ , where  $a_k$  are the limits obtained in *Step 1*. We have that

$$\begin{aligned} \|\mathbf{R}_{\delta_n}(\hat{\nu}_{\delta_n})\|_F^2 &= \sum_{i,j=1}^M \left\langle g_i, \left( -V_{\delta_n} - \sum_{k=1}^p \Lambda'(\lambda_0, \mu_0)(\tau \hat{a}_{k,\delta_n} \chi_k, \hat{a}_{k,\delta_n} \chi_k) \right) g_j \right\rangle^2, \\ \|\mathbf{R}(\nu)\|_F^2 &= \sum_{i,j=1}^M \left\langle g_i, \left( -V - \sum_{k=1}^p \Lambda'(\lambda_0, \mu_0)(\tau a_k \chi_k, a_k \chi_k) \right) g_j \right\rangle^2. \end{aligned}$$

With the same arguments as in the proof of Theorem 3.8 in [9], we are led to

$$\|\mathbf{R}(\nu)\|_F \leq \|\mathbf{R}(\hat{\nu})\|_F.$$

Further on, by the uniqueness of the minimizer we obtain  $\nu = \hat{\nu}$  that is

$$a_k = \hat{a}_k = \begin{cases} 0 & \text{for } \mathcal{B}_k \not\subseteq \mathcal{D}, \\ a_{\max} & \text{for } \mathcal{B}_k \subseteq \mathcal{D}. \end{cases}$$

*Step 4: Convergence of the whole sequence  $\hat{\nu}_\delta$*

Again this is obtained in the same way as in [9].  $\square$

*Remark 4.14.* All in all, we are led to the discrete formulation of the minimization problem for noisy data:

$$(4.16) \quad \min_{\nu \in \mathcal{C}_\delta} \|\mathbf{R}_\delta(\nu)\|_F,$$

under the constraint

$$(4.17) \quad 0 \leq \nu_k \leq \min \left( a_{\max}, \tilde{\beta}_{k,\delta} \right),$$

where

$$(4.18) \quad a_{\max} = \mu_0 - \frac{\mu_0^2}{\mu_0 + c^\mu},$$

$$(4.19) \quad \tau = \frac{1}{a_{\max}} \left( \lambda_0 - \frac{\lambda_0^2}{\lambda_0 + c^\lambda} \right),$$

$$(4.20) \quad \tilde{\beta}_{k,\delta} = \max \{ a \geq 0 : -a \mathbf{S}_k^\tau \geq -\delta \mathbf{I} - |\mathbf{V}^\delta| \}$$

with  $|\mathbf{V}^\delta| := \sqrt{(\mathbf{V}^\delta)^* \mathbf{V}^\delta}$ .

Next, we take a closer look at the determination of  $\tilde{\beta}_{k,\delta}$  (see [9]), where  $\tilde{\beta}_{k,0} = \tilde{\beta}_k$ :

First, we replace the infinite-dimensional operators  $|V^\delta|$  and  $\Lambda'(\lambda_0, \mu_0)$  by the  $M \times M$  matrices  $\mathbf{V}^\delta, \mathbf{S}_k^\tau$  such that we need to find  $\tilde{\beta}_{k,\delta}$  with

$$-a \mathbf{S}_k^\tau \geq -\delta \mathbf{I} - |\mathbf{V}^\delta|$$

for all  $a \in [0, \tilde{\beta}_{k,\delta}]$ . Due to the fact that  $\delta \mathbf{I} + |\mathbf{V}^\delta|$  is a Hermitian positive-definite matrix, the Cholesky decomposition allows us to decompose it into the product of a lower triangular matrix and its conjugate transpose, i.e.

$$\delta \mathbf{I} + |\mathbf{V}^\delta| = \mathbf{L} \mathbf{L}^T.$$

We want to remark that this decomposition is unique. In addition,  $\mathbf{L}$  is invertible, since

$$0 < \det(\delta \mathbf{I} + \mathbf{V}^\delta) = \det(\mathbf{L}) \det(\mathbf{L}^T) = \det(\mathbf{L}) \overline{\det(\mathbf{L})}.$$

For each  $a > 0$ , it follows that

$$-a \mathbf{S}_k^\tau + \delta \mathbf{I} + |\mathbf{V}^\delta| = -a \mathbf{S}_k^\tau + \mathbf{L} \mathbf{L}^T = \mathbf{L} (-a \mathbf{L}^{-1} \mathbf{S}_k^\tau (\mathbf{L}^T)^{-1} + \mathbf{I}) \mathbf{L}^T.$$

It should be noted that in this notation  $\tilde{\beta}_{k,M,\delta} = \tilde{\beta}_{k-M,\delta}$  for  $k = M+1, \dots, 2M$ .

Based on this, we go over to the consideration of the eigenvalues and apply Weyl's Inequality. Since the positive semi-definiteness of  $-a \mathbf{S}_k^\tau + \delta \mathbf{I} + |\mathbf{V}^\delta|$  is equivalent to the positive semi-definiteness of  $a \mathbf{L}^{-1} \mathbf{S}_k^\tau (\mathbf{L}^T)^{-1} + \mathbf{I}$ , we obtain

$$\theta_j(-a \mathbf{L}^{-1} \mathbf{S}_k^\tau (\mathbf{L}^T)^{-1} + \mathbf{I}) = a \theta_j(-\mathbf{L}^{-1} \mathbf{S}_k^\tau (\mathbf{L}^T)^{-1}) + 1, \quad j = 1, \dots, M,$$

where  $\theta_1(A) \geq \dots \geq \theta_M(A)$  denote the  $M$ -eigenvalues of some matrix  $A$ .

Further, let  $\bar{\theta}_M(\mathbf{L}^{-1} \mathbf{S}_k^\tau (\mathbf{L}^T)^{-1})$  be the smallest eigenvalue of the matrix  $\mathbf{L}^{-1} \mathbf{S}_k^\tau (\mathbf{L}^T)^{-1}$ . Since  $\mathbf{S}_k^\tau$  is positive semi-definite, so is  $\mathbf{L}^{-1} \mathbf{S}_k^\tau (\mathbf{L}^T)^{-1}$ . Thus,  $\bar{\theta}_M(\mathbf{L}^{-1} \mathbf{S}_k^\tau (\mathbf{L}^T)^{-1}) \leq 0$ . Following the lines of [9], we obtain

$$\tilde{\beta}_{k,\delta} = -\frac{1}{\bar{\theta}_M(\mathbf{L}^{-1} \mathbf{S}_k^\tau (\mathbf{L}^T)^{-1})} \geq 0.$$

**4.2.3. Numerical Realization.** We close this section with a numerical example, where we again consider two inclusions (tumors) in a biological tissue as shown in Figure 1 (for the values of the Lamé parameter see Table 1). In addition to the Lamé parameters, we use the estimated lower and upper bounds  $c^\lambda, c^\mu, C^\lambda, C^\mu$  given in Table 2.

	$\gamma^\lambda$	$\gamma^\mu$
lower bounds	$c^\lambda = 1.2 \cdot 10^6$	$c^\mu = 1.2 \cdot 10^4$
upper bounds	$C^\lambda = 1.7 \cdot 10^6$	$C^\mu = 1.7 \cdot 10^4$

TABLE 2  
Lower and upper bounds  $c^\lambda, c^\mu, C^\lambda, C^\mu$  in [Pa].

For the implementation, we again consider difference measurements and apply quadprog from Matlab in order to solve the minimization problem.

**Exact Data.** We start with exact data, i.e. data without noise and due to the definition of  $\delta$  given in (3.8), with  $\delta = 0$ .

Figure 11 presents the results as 3D plots, while Figure 12 shows the corresponding cuts for  $\mu$ . For the same reasons as discussed in Section 3, we change the transparency of the plots of the 3D reconstruction of Figure 11 as indicated in Figure 10. Thus, tetrahedrons with low values have a higher transparency, whereas tetrahedrons with large values are plotted opaque.

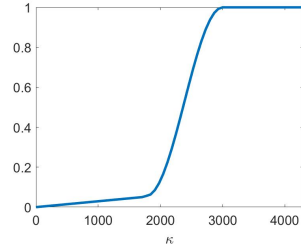


FIG. 10. Transparency function for the plots in Figure 11 mapping the values of  $\kappa$  to  $\alpha(\kappa)$ .

Figures 11 - 12 show that solving the minimization problem (4.16) indeed yields a detection and reconstruction with respect to both Lamé parameters  $\mu$  and  $\lambda$ .

*Remark 4.15.* Compared with the results obtained with the one-step linearization method as depicted in Figure 3 (right hand side), this is an improvement because we are now able to also obtain information concerning  $\lambda$  which is not possible with the heuristic approach considered in (3.6).

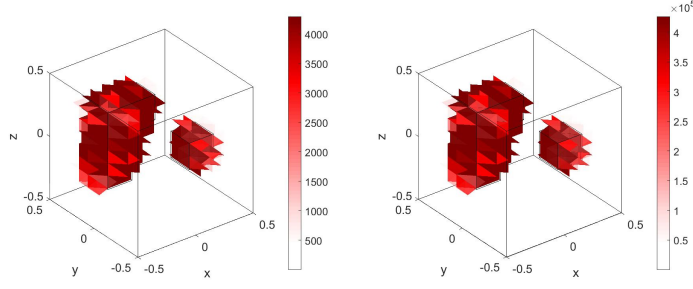


FIG. 11. Shape reconstruction of two inclusions (red) of the reconstructed difference in the Lamé parameter  $\mu$  (left hand side) and  $\lambda$  (right hand side) without noise,  $\delta = 0$  and transparency function  $\alpha$  as shown in Figure 10.

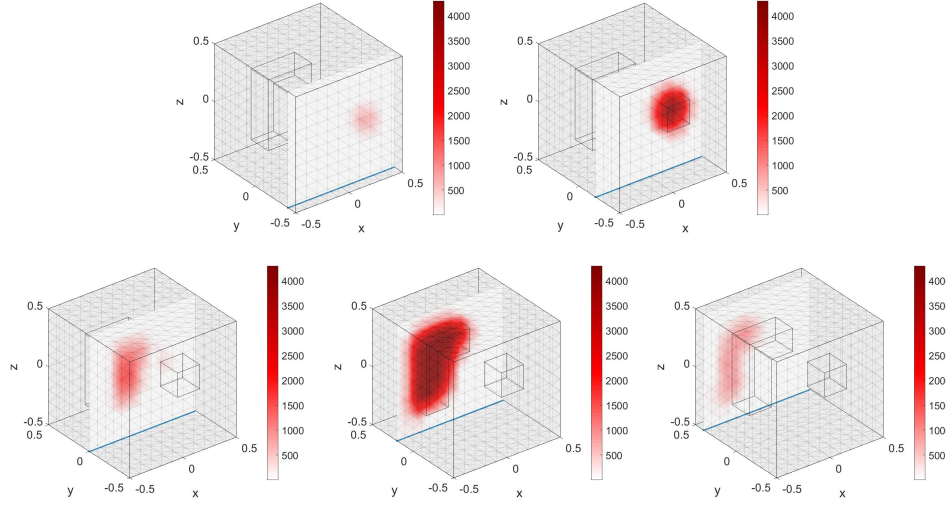


FIG. 12. Shape reconstruction of two inclusions (red) of the reconstructed difference in the Lamé parameter  $\mu$  depicted as cuts without noise and  $\delta = 0$ .

**Noisy Data.** Finally, we take a look at noisy data with a relative noise level  $\eta = 10\%$ , where the  $\delta$  is determined as given in (3.8).

Figures 13 - 14 document that we can even reconstruct the inclusions for noisy data which is a huge advantage compared with the results of the one-step linearization (see Figure 7- 8). This shows us, that the numerical simulations based on the monotonicity-based regularization are only marginally affected by noise as we have proven in theory, e.g., in Theorem 4.9.

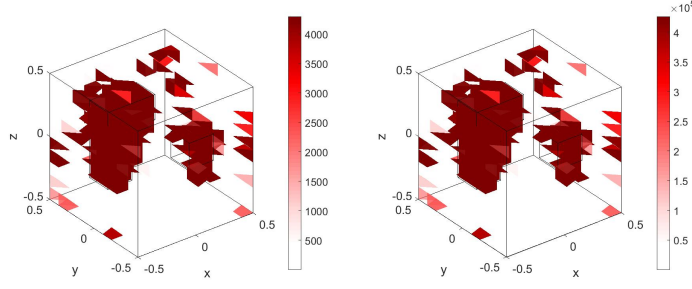


FIG. 13. Shape reconstruction of two inclusions (red) of the reconstructed difference in the Lamé parameter  $\mu$  (left hand side) and  $\lambda$  (right hand side) with relative noise  $\eta = 10\%$ ,  $\delta = 8.3944 \cdot 10^{-8}$  and transparency function  $\alpha$  as shown in Figure 10.

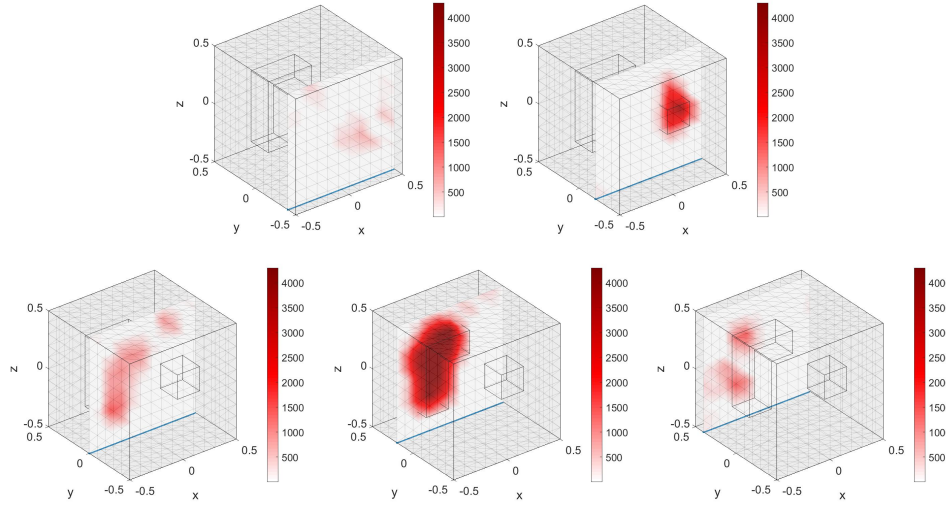


FIG. 14. Shape reconstruction of two inclusions (red) of the reconstructed difference in the Lamé parameter  $\mu$  depicted as cuts with relative noise  $\eta = 10\%$  and  $\delta = 8.3944 \cdot 10^{-8}$ .

**5. Summary.** In this paper we introduced a standard one-step linearization method applied to the Neumann-to-Dirichlet operator as a heuristical approach and a monotonicity-based regularization for solving the resulting minimization problem. In addition, we proved the existence of such a minimizer. Finally, we presented numerical examples.

**Appendix.** For the monotonicity-based regularization we focused on the case  $\lambda \geq \lambda_0$ ,  $\mu \geq \mu_0$  (see Section 5). For sake of completeness, we formulate the corresponding results for the case that  $\lambda \leq \lambda_0$ ,  $\mu \leq \mu_0$ . Thus, we summarize the corresponding main results and define the set

$$\mathcal{C} := \left\{ \nu \in L_+^\infty(\Omega) : \nu = \sum_{k=1}^p a_k \chi_k, a_k \in \mathbb{R}, 0 \geq a_k \geq -\min(a_{\max}, \beta_k) \right\}$$

where the quantities  $a_{\max}$  and  $\tau_{\max}$  are defined as

$$(5.1) \quad a_{\max} := c^\mu \quad \text{and} \quad \tau := \frac{c^\lambda}{c^\mu},$$

such that

$$(5.2) \quad -2(\mu - \mu_0) + 2a \geq 0,$$

$$(5.3) \quad -(\lambda - \lambda_0) + \tau a \geq 0$$

for all  $0 \geq a \geq -a_{\max}$ .

*Remark 5.1.* The value  $a_{\max}$  is obtained from the estimates in Lemma 4.1 which results in a different upper bound  $a$  compared with the case  $\lambda \geq \lambda_0, \mu \geq \mu_0$ .

Thus, the theorem for exact data is given by

THEOREM 5.2. *Consider the minimization problem*

$$(5.4) \quad \min_{\nu \in \mathcal{C}} \|\mathbf{R}(\nu)\|_F.$$

The following statements hold true:

- (i) Problem (5.4) admits a unique minimizer  $\hat{\nu}$ .
- (ii)  $\text{supp}(\hat{\nu})$  and  $\mathcal{D}$  agree up to the pixel partition, i.e. for any pixel  $\mathcal{B}_k$

$$\mathcal{B}_k \subset \text{supp}(\hat{\nu}) \quad \text{if and only if} \quad \mathcal{B}_k \subset \mathcal{D}.$$

Moreover,

$$\hat{\nu} = \sum_{\mathcal{B}_k \subseteq \mathcal{D}} a_{\max} \chi_k.$$

The corresponding results for noisy data is formulated in the following theorem, where  $\mathbf{R}_\delta(\nu)$  represents the matrix  $(\langle g_i, r_\delta(\nu) g_j \rangle)_{i,j=1,\dots,M}$  and the admissible set for noisy data is defined by

$$\mathcal{C}_\delta := \left\{ \nu \in L_+^\infty(\Omega) : \nu = \sum_{k=1}^p a_k \chi_k, a_k \in \mathbb{R}, 0 \geq a_k \geq -\min(a_{\max}, \beta_{k,\delta}) \right\}.$$

THEOREM 5.3. *Consider the minimization problem*

$$(5.5) \quad \min_{\nu \in \mathcal{C}_\delta} \|\mathbf{R}_\delta(\nu)\|_F.$$

The following statements hold true:

- (i) Problem (5.5) admits a minimizer.
- (ii) Let  $\hat{\nu} = \sum_{\mathcal{B}_k \subseteq \mathcal{D}} a_{\max} \chi_k$  be the minimizer of (5.4) and  $\hat{\nu}_\delta = \sum_{k=1}^p a_{k,\delta} \chi_k$  of problem (5.5), respectively. Then  $\hat{\nu}_\delta$  converges pointwise and uniformly to  $\hat{\nu}$  as  $\delta$  goes to 0.

## REFERENCES



- [1] S. ANDRIEUX, A. ABDA, AND H. BUI, *Reciprocity principle and crack identification*, Inverse Problems, 15 (1999), pp. 59–65.
- [2] E. BERETTA, E. FRANCINI, A. MORASSI, E. ROSSET, AND S. VESSELLA, *Lipschitz continuous dependence of piecewise constant Lamé coefficients from boundary data: the case of non-flat interfaces*, Inverse Problems, 30 (2014), p. 125005.
- [3] E. BERETTA, E. FRANCINI, AND S. VESSELLA, *Uniqueness and Lipschitz stability for the identification of Lamé parameters from boundary measurements*, Inverse Problems & Imaging, 8 (2014), pp. 611–644.
- [4] P. G. CIARLET, *The finite element method for elliptic problems*, North Holland, 1978.
- [5] S. EBERLE AND B. HARRACH, *Shape reconstruction in linear elasticity: Standard and linearized monotonicity method*, Inverse Problems, 37 (2021), p. 045006.
- [6] S. EBERLE, B. HARRACH, H. MEFTAH, AND T. REZGUI, *Lipschitz stability estimate and reconstruction of Lamé parameters in linear elasticity*, Inverse Problems in Science and Engineering, 29 (2021), pp. 396–417.
- [7] G. ESKIN AND J. RALSTON, *On the inverse boundary value problem for linear isotropic elasticity*, Inverse Problems, 18 (2002), p. 907.
- [8] R. FERRIER, M. KADRI, AND P. GOSSELET, *Planar crack identification in 3D linear elasticity by the reciprocity gap method*, Computer Methods in Applied Mechanics and Engineering, 355 (2019), pp. 193–215.
- [9] B. HARRACH AND N. MACH, *Enhancing residual-based techniques with shape reconstruction features in electrical impedance tomography*, Inverse Problems, 32 (2016).
- [10] B. HARRACH AND M. ULLRICH, *Monotonicity-based shape reconstruction in electrical impedance tomography*, SIAM Journal on Mathematical Analysis, 45 (2013), pp. 3382–3403.
- [11] S. HUBMER, E. SHERINA, A. NEUBAUER, AND O. SCHERZER, *Lamé parameter estimation from static displacement field measurements in the framework of nonlinear inverse problems.*, SIAM Journal on Imaging Sciences, 11 (2018), pp. 1268–1293.
- [12] M. IKEHATA, *Inversion formulas for the linearized problem for an inverse boundary value problem in elastic prospection*, SIAM Journal on Applied Mathematics, 50 (1990), pp. 1635–1644.
- [13] O. Y. IMANUVILOV AND M. YAMAMOTO, *On reconstruction of Lamé coefficients from partial Cauchy data*, Journal of Inverse and Ill-posed Problems, 19 (2011), pp. 881–891.
- [14] B. JADAMBA, A. KHAN, AND F. RACITI, *On the inverse problem of identifying Lamé coefficients in linear elasticity*, Computers and Mathematics with Applications, 56 (2008), pp. 431–443.
- [15] Y.-H. LIN AND G. NAKAMURA, *Boundary determination of the Lamé moduli for the isotropic elasticity system*, Inverse Problems, 33 (2017), p. 125004.
- [16] L. MARIN AND D. LESNIC, *Regularized boundary element solution for an inverse boundary value problem in linear elasticity*, Communications in Numerical Methods in Engineering, 18 (2002), pp. 817–825.
- [17] L. MARIN AND D. LESNIC, *Boundary element-Landweber method for the Cauchy problem in linear elasticity*, IMA Journal of Applied Mathematics, 70 (2005), pp. 323–340.
- [18] G. NAKAMURA, K. TANUMA, AND G. UHLMANN, *Layer stripping for a transversely isotropic elastic medium*, SIAM Journal on Applied Mathematics, 59 (1999), pp. 1879–1891.
- [19] G. NAKAMURA AND G. UHLMANN, *Identification of Lamé parameters by boundary measurements*, American Journal of Mathematics, (1993), pp. 1161–1187.
- [20] G. NAKAMURA AND G. UHLMANN, *Inverse problems at the boundary for an elastic medium*, SIAM journal on mathematical analysis, 26 (1995), pp. 263–279.
- [21] G. NAKAMURA AND G. UHLMANN, *Global uniqueness for an inverse boundary value problem arising in elasticity*, Inventiones mathematicae, 152 (2003), pp. 205–207.
- [22] A. OBERAI, N. GOKHALE, M. DOYLEY, AND J. BAMBER, *Evaluation of the adjoint equation based algorithm for elasticity imaging*, Physics in Medicine and Biology, 49 (2004), pp. 2955–2974.
- [23] A. OBERAI, N. GOKHALE, AND G. FEIJOO, *Solution of inverse problems in elasticity imaging using the adjoint method*, Inverse Problems, 19 (2003), pp. 297–313.
- [24] D. SEIDL, A. OBERAI, AND P. BARBONE, *The coupled adjoint-state equation in forward and inverse linear elasticity: Incompressible plane stress*, Computer Methods in Applied Mechanics and Engineering, 357 (2019), p. 112588.
- [25] P. STEINHORST AND A. SÄNDIG, *Reciprocity principle for the detection of planar cracks in anisotropic elastic material*, Inverse Problems, 29 (2012), p. 085010.
- [26] A. TAMBURRINO, *Monotonicity based imaging methods for elliptic and parabolic inverse problems*, J. Inverse Ill-Posed Probl., 14 (2006), pp. 633–642.
- [27] A. TAMBURRINO AND G. RUBINACCI, *A new non-iterative inversion method for electrical resistance tomography*, Inverse Problems, 18 (2002), p. 1809.